



# Optics Letters

## Compensating spatially dependent dispersion in visible light OCT

AARON KHO<sup>1</sup> AND VIVEK J. SRINIVASAN<sup>1,2,\*</sup>

<sup>1</sup>Department of Biomedical Engineering, University of California, Davis, California 95616, USA

<sup>2</sup>Department of Ophthalmology and Vision Science, University of California Davis School of Medicine, Sacramento, California 96817, USA

\*Corresponding author: vjsriniv@ucdavis.edu

Received 29 November 2018; revised 5 January 2019; accepted 6 January 2019; posted 7 January 2019 (Doc. ID 351962); published 4 February 2019

**Visible light optical coherence tomography (OCT) has recently emerged in retinal imaging, with claims of micrometer-scale axial resolution and multi-color (sub-band) imaging. Here, we show that the large dispersion of optical glass and aqueous media, together with broad optical bandwidths often used in visible light OCT, compromises both of these claims. To rectify this, we introduce the notion of spatially dependent (i.e., depth and transverse position-dependent) dispersion. We use a novel sub-band, sub-image correlation algorithm to estimate spatially dependent dispersion in our 109 nm bandwidth visible light OCT mouse retinal imaging system centered at 587 nm. After carefully compensating spatially dependent dispersion, we achieve delineation of fine outer retinal bands in mouse strains of varying pigmentation. Spatially dependent dispersion correction is critical for broader bandwidths and shorter visible wavelengths.** © 2019 Optical Society of America

<https://doi.org/10.1364/OL.44.000775>

Recently, visible light optical coherence tomography (OCT) has emerged for ultrahigh resolution and multi-color functional imaging in biological tissues [1–3]. In the retina, visible light OCT potentially offers micrometer ( $\mu\text{m}$ )-scale axial resolution and the intriguing ability to perform depth-resolved, multi-color retinal imaging with the same wavelengths of light that initiate visual phototransduction. However, visible light OCT poses many technical challenges, such as limited exposures [4] and photon counts, high light scattering and absorption [2], excess noise in light sources [5], and chromatic aberrations [3]. By addressing some of these challenges, recent research is beginning to realize the potential of visible light OCT [3].

In ray optics, dispersion refers to a variation in the refractive index of a material with wavelengths. In OCT, as in ultrafast optics, chromatic dispersion typically refers to a nonlinear variation in the spectral phase delay versus optical frequency [6]. By either definition, dispersion is more severe for optical glass and aqueous media at visible wavelengths, as compared to near-infrared (NIR) wavelengths normally used for retinal OCT. Material dispersion is a root cause of chromatic aberration, which was previously assessed [3]. However, dispersion of

the spectral phase has not been thoroughly analyzed in visible light OCT. To our knowledge, visible light OCT studies to date compensated depth-independent dispersion (DID) [7] using either physical or numerical means, or a combination thereof. In visible light OCT, depth-dependent dispersion (DDD) has not been analyzed, though it has been considered at longer OCT wavelengths [8]. In this Letter, to fully manage dispersion in visible light OCT, we introduce the concept of spatially dependent dispersion (SDD), which includes both depth and transverse variations, the latter of which has not been previously treated. We present a novel, automated numerical approach, based on sub-band, sub-image correlation, to measure and correct SDD. Our results show that  $\mu\text{m}$ -scale image resolution and accurate multi-color imaging with visible light OCT requires accounting for SDD.

To treat dispersion simply, we approximate the visible OCT wavefront as planar, neglecting curvature and the Gouy phase shift. For double-pass propagation through a material with length  $z$ , the spectral phase delay of a plane wave is given by

$$\phi(\omega, z) = 2k(\omega) \times z = 2 \frac{\omega n(\omega)}{c} \times z, \quad (1)$$

where  $k(\omega)$  is the material propagation constant,  $n(\omega)$  is the material refractive index [e.g., Fig. 1(A)],  $\omega$  is optical angular frequency, and  $c$  is the speed of light in free space. As described previously [6],  $k(\omega)$  can be decomposed into constant, linear, and nonlinear terms, with subscripts “0,” “L,” and “NL,” respectively, based on a Taylor series at center frequency  $\omega_0$ :

$$\begin{aligned} k(\omega) &= k_0 + k_L(\omega) + k_{\text{NL}}(\omega) \\ &= k_0 + \left. \frac{dk}{d\omega} \right|_{\omega_0} (\omega - \omega_0) + \sum_{m=2}^{\infty} \frac{1}{m!} \left. \frac{d^m k}{d\omega^m} \right|_{\omega_0} (\omega - \omega_0)^m. \end{aligned} \quad (2)$$

The constant term in Eq. (2), with units of radians (rad)/ $\mu\text{m}$ , is the propagation constant at  $\omega_0$ , related to the reciprocal of the phase velocity [ $k_0 = k(\omega_0) = \omega_0/v_{p,0}$ ]. The coefficient of the linear term, with units of femtoseconds (fs)/ $\mu\text{m}$ , is the reciprocal of the group velocity [ $k'(\omega_0) = 1/v_{g,0}$ ]. The coefficient of the quadratic ( $m = 2$ ) term, with units of  $\text{fs}^2/\mu\text{m}$ , is half the group velocity dispersion [ $\text{GVD}/2 = k''(\omega_0)/2$ ].

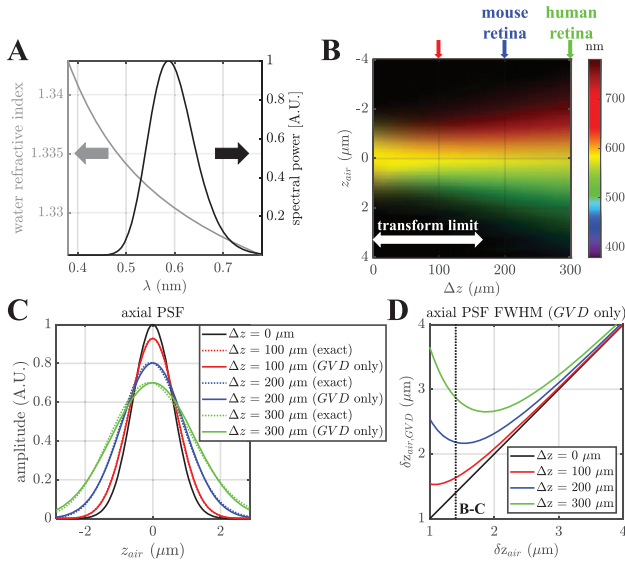


**Fig. 1.** Simulations based on Eqs. (1)–(6) show the severity of depth-dependent (DD) dispersion in our visible light OCT system ( $\lambda_0 = 587$  nm,  $\delta\lambda = 109$  nm). A: water refractive index and Gaussian spectrum versus wavelength. B: simulated axial point spread function (PSF) broadens with increasing axial depth ( $\Delta z$ ). The PSF phase slope is encoded as the visible color of the corresponding wavelength. C: the magnitude of the PSF (dotted lines) is well-predicted by group velocity dispersion (GVD) alone (solid lines), while higher dispersion orders induce PSF asymmetry. D: PSF broadening with depth [Eq. (7)] due to GVD (colored solid lines) increases as the transform limited resolution (solid black line) is improved. For our system parameters, water dispersion severely degrades resolution (dotted black line).

GVD implies a change in group velocity with frequency, which causes group delay dispersion (GDD), after propagation through the material over a distance of  $2z$  [ $GDD = GVD \times 2z$ ]. GDD, with units of  $\text{fs}^2$ , results in temporal spreading of a short pulse with many wavelengths. Higher-order nonlinear terms ( $m > 2$ ) also contribute to the degree of spreading. In OCT, the spectral phase *mismatch* between the sample and reference arms, each containing materials with different lengths and propagation constants, comprises three terms, each corresponding with a term in Eq. (2):

$$\Delta\phi(\omega, \Delta z) = \Delta\phi_0(\Delta z) + \Delta\phi_L(\omega, \Delta z) + \Delta\phi_{NL}(\omega, \Delta z). \quad (3)$$

Assuming, henceforth, that  $k$  in Eq. (2) applies to the sample propagation constant, we now study the depth dependence of each term in Eq. (3). The constant phase term  $\Delta\phi_0(\Delta z) = \Delta\Phi_0 + 2k_0\Delta z$  comprises both a depth-independent (DI) part ( $\Delta\Phi_0$ ) and a depth-dependent (DD) part. By definition, the linear phase term  $\Delta\phi_L(\omega, \Delta z) = 2k_L(\omega)\Delta z = 2/v_{g,0} \times (\omega - \omega_0)\Delta z$  is DD. The dispersive nonlinear phase term

$$\Delta\phi_{NL}(\omega, \Delta z) = \Delta\Phi_{NL}(\omega) + 2k_{NL}(\omega)\Delta z \quad (4)$$

includes a DI part, with an assumed Taylor expansion of  $\Delta\Phi_{NL}(\omega) = \sum_{m=2}^{\infty} a_m(\omega - \omega_0)^m$ , and a DD part. The DI part arises from dispersive mismatch between the reference arm and sample arm at zero delay ( $\Delta z = 0$ ). Specifically, the  $m = 2$  term describes GVD mismatch. To understand DID and DDD, we consider the OCT axial point spread function (PSF), neglecting mirror terms, for a reflector at depth  $\Delta z$ :

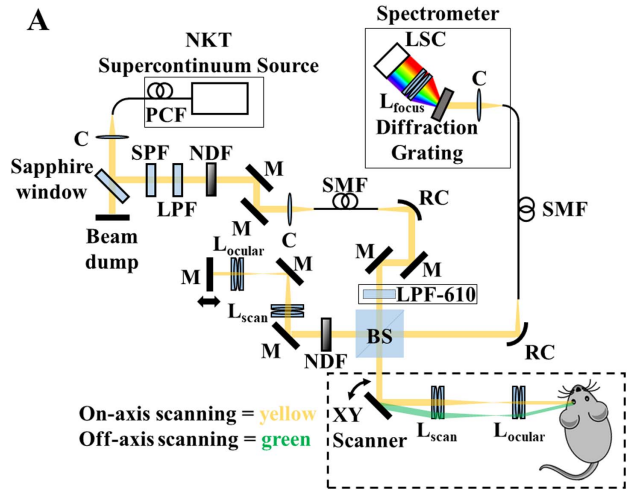


**Fig. 2.** Visible light OCT ophthalmoscope schematic. Differences in material traversed by the beam when scanning off axis (green) lead to transverse dependence of dispersion. (L, lens; SPF, short pass filter; LPF, long pass filter; NDF, neutral density filter; M, mirror; LSC, line scan camera; C, collimator; RC, reflective collimator; SMF, single mode fiber; BS, beam splitter; PCF, photonic crystal fiber; LPF-610, 610 nm long pass filter for alignment purposes.)

$$\begin{aligned} s(\tau, \Delta z) &= \mathcal{F}^{-1}\{I(\omega - \omega_0) \exp[i\Delta\phi(\omega, \Delta z)]\} \\ &= e^{i\Delta\phi_0(\Delta z)} \gamma(\tau - 2\Delta z/v_{g,0}) * \mathcal{F}^{-1}\{e^{i\Delta\phi_{NL}(\omega, \Delta z)}\}, \end{aligned} \quad (5)$$

where  $\mathcal{F}^{-1}\{\}$  represents an inverse Fourier transform with respect to  $\omega - \omega_0$  to time lag  $\tau$ , and  $*$  denotes convolution in  $\tau$ .  $I(\omega - \omega_0)$  represents the interference spectrum amplitude, whose inverse Fourier transform, the mutual coherence function  $\gamma(\tau) = \mathcal{F}^{-1}\{I(\omega - \omega_0)\}$ , is the transform limited PSF, with no nonlinear phase and optimal resolution. Through the convolution in Eq. (5), the nonlinear phase  $\Delta\phi_{NL}$  causes a broadening of the PSF. If both DID and DDD have the same sign, DID causes uniform broadening irrespective of  $\Delta z$ , while DDD causes a broadening that depends on  $\Delta z$ . In most OCT systems, the depth dependence of  $\Delta\phi_{NL}$  can be neglected, i.e.,  $2k_{NL}(\omega)\Delta z \ll \pi$  for all  $\omega$  and  $\Delta z$  of interest.

The effect of the linear phase in Eq. (3) is to shift the coherence function in Eq. (5) along the time lag axis to  $\tau = 2\Delta z/v_{g,0}$ . The last essential step to consider is rescaling the PSF axis from time lag  $\tau$  to axial position or depth  $z_{\text{img}}$ , assuming a group velocity  $v_{g,\text{img}}$ :

$$\text{psf}(z_{\text{img}}, \Delta z) = s(\tau, \Delta z)|_{\tau=2z_{\text{img}}/v_{g,\text{img}}}. \quad (6)$$

Note that  $v_{g,\text{img}}$  need not necessarily equal  $v_g$  for the sample. For instance,  $\text{psf}(z_{\text{air}}, \Delta z)$  can be obtained by assuming  $v_{g,\text{img}} = c$  or  $\tau = 2z_{\text{air}}/c$  in Eq. (6). Simulations (Fig. 1) based on applying the above theory with  $n(\omega)$  for water [9] clearly confirm that DDD degrades resolution in visible light OCT, even for thin specimens such as the retina ( $\Delta z \sim 200$ – $300$   $\mu\text{m}$ ). To obtain a simple analytical expression that explains this unexpected finding, we next consider the expansion of  $\Delta\phi_{NL}$  in Eq. (5) up to the GVD term, which dominates higher dispersion orders ( $m > 2$ ) for aqueous media [Fig. 1(C)] at visible wavelengths.

Considering just second-order (GVD) effects, we observe that (1) GVD of aqueous media in the visible range is twice that in

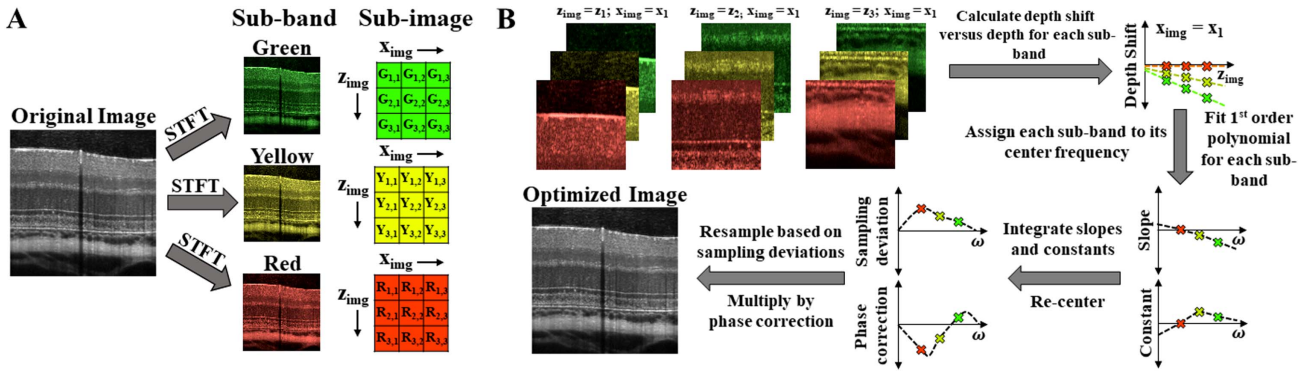


**Fig. 3.** Correcting SDD using a sub-band, sub-image correlation algorithm. A: via short time Fourier transform (STFT), the original image is split into spectral sub-band images, which are further partitioned into sub-images. B: for each sub-image, each sub-band is correlated to a reference sub-band, resulting in a relative depth shift for each sub-band versus image depth. For each transverse position ( $x_{\text{img}} = x_1$  shown) and sub-band, the shift with depth is fit by a first-order polynomial with the  $y$  intercept (constant) and first-order (slope) terms relating to depth-independent (DI) and DD dispersion, respectively. Assigning parameters to the center frequency for each sub-band and center transverse position for each sub-image, we can interpolate to find the constants and slopes for every frequency ( $\omega$ ) and transverse position. Integration of the slopes and constants yields the cumulative sampling deviation and phase correction. To avoid depth scaling or shifting of the image, a re-centering procedure is included. Correction is achieved by complex phase correction and resampling based on the sampling deviation.

the NIR, exacerbating the effects of spatially dependent GDD [9]. (2) Practitioners of visible light OCT typically use large optical frequency bandwidths ( $\sim \delta\lambda/\lambda_0^2$ ) for spectroscopy or ultra-high axial resolution. (3) The degradation of axial resolution by GDD worsens as the bandwidth increases [Fig. 1(D)]. Specifically, if  $I(\omega - \omega_0)$  is Gaussian, the GVD-degraded image resolution based on Eqs. (5) and (6) is readily derived:

$$\delta z_{\text{img,GVD}} = \delta z_{\text{img}} \sqrt{1 + \frac{(2 \log 2)^2 v_{g,\text{img}}^4 \text{GDD}^2}{\delta z_{\text{img}}^4}}, \quad (7)$$

where  $\delta z_{\text{img}} = 2 \log 2 \lambda_0^2 / (\pi n_{g,\text{img}} \delta\lambda)$  is the theoretical transform limited resolution in terms of the full width at half-maximum (FWHM) wavelength bandwidth ( $\delta\lambda$ ), group refractive index ( $n_{g,\text{img}} = c/v_{g,\text{img}}$ ), and center wavelength ( $\lambda_0 = 2\pi/k_0$ ). From Eq. (7), we can infer that GDD degrades resolution when  $\delta z_{\text{img,GVD}} \geq \delta z_{\text{img}} \sqrt{2}$  or  $\delta z_{\text{img}} \leq v_{g,\text{img}} \sqrt{2 \log 2} \times \text{GDD}$ . If dispersion is matched at the internal limiting membrane (ILM) depth, since  $\lambda_0 = 587 \text{ nm}$  and  $\text{GDD} = \text{GVD} \times 2\Delta z$ , where  $\text{GVD} = 0.047 \text{ fs}^2/\mu\text{m}$  [9] and  $\Delta z \sim 200(300) \mu\text{m}$  for the mouse (human) retina, we obtain from Eq. (7) the guideline that axial resolution is degraded at the posterior retina by GDD, and DDD compensation is needed if  $\delta\lambda \gtrsim 99(80) \text{ nm}$ . Shorter central wavelengths result in higher GVD and even more stringent criteria. Thus, in ultrahigh resolution OCT, if DID and DDD have the same sign, DID causes a DI resolution degradation, while DDD causes a DD resolution degradation that worsens with increasing  $\Delta z$ .

The effects of dispersion must also be considered in spectroscopic OCT, where the interference spectrum is divided into sub-bands. For instance, consider a sub-band with a center wavelength of  $\omega_0 + \delta\omega_0$ . Assuming again that sub-bands are narrow and the GVD term dominates higher-order terms ( $m > 2$ ), the main effect of dispersion is to modify the spectral phase slope in the sub-band. All Taylor expansions about  $\omega_0 + \delta\omega_0$  are performed, as opposed to  $\omega_0$ , and the linear phase term yielding a shift in the apparent PSF depth from  $\Delta z$  to  $\Delta z \times v_{g,0}/v_{g,s} + a_2 v_{g,0} \delta\omega_0$  is considered, where  $v_{g,s}$  is the sub-band group

velocity. Accounting for the rescaling operation in Eq. (6) with  $v_{g,\text{img}} = v_{g,0}$  yields a depth scaling of the sub-band image by  $v_{g,0}/v_{g,s} \approx 1 + k''(\omega_0) v_{g,0} \delta\omega_0$  relative to the central sub-band, followed by a shift of the sub-band image by  $\sim a_2 v_{g,0} \delta\omega_0$ , where  $\delta\omega_0 = \omega_s - \omega_0$  is the sub-band offset relative to the central frequency [10]. A positive GVD corresponds to a stretch of higher frequency sub-band images, since the actual group velocity is smaller than assumed in image reconstruction [Eq. (6)]. Thus, in spectroscopic OCT, DID causes a sub-band shift, while DDD causes a scaling (stretch or compression) of the sub-band depth axis.

A spectral/Fourier domain OCT ophthalmoscope for *in vivo* murine retinal imaging was built [Fig. 2] with a supercontinuum light source (EXW-12, NKT Photonics A/S, Denmark). The scan and tube lenses were achromatic doublet pairs with 150 and 30 mm effective focal lengths, respectively, to achieve a beam diameter of 200  $\mu\text{m}$  at the cornea (effective NA = 0.04) to mitigate aberrations. All sample arm lenses were matched with identical lenses in the reference arm. The spectrometer was calibrated using a previously described procedure [11]. Our theoretical depth resolution in air (tissue) was 1.4 (1.0)  $\mu\text{m}$ . Imaging was performed with a 10 kHz line rate and 300  $\mu\text{W}$  power at the cornea over a transverse angle of  $26^\circ$  with 350–700 axial scans. Due to the high visible light dispersion of common optical glasses, for which GVD is 2–3 times larger than for NIR light, and aqueous media [9], discussed previously, as well as the fact that the OCT beam sees different material thicknesses as the beam is scanned [Fig. 2], we explicitly allow for the possibility that DID depends on a transverse position [i.e.,  $a_m \rightarrow a_m(x)$  in the Taylor expansion of  $\Delta\Phi_{\text{NL}}$ ]. Transverse and DDD, together, constitute SDD.

The spectral phase of a specular reflection can be used to determine dispersion [8,12]. However, specular reflections are not available at multiple spatial positions in an image. Here, we take advantage of the laminar retinal structure, which yields distinct layers in sub-band sub-images (Fig. 3). If dispersion is well-compensated, these layers must align in all sub-bands at all transverse positions and depths. Thus, we

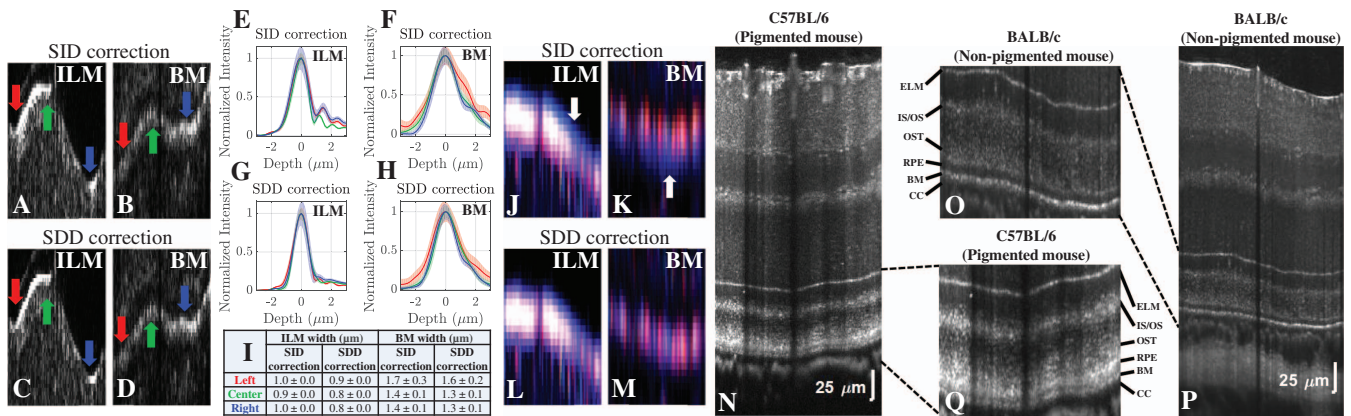


**Fig. 4.** A–D: zooms of visible light OCT images of the ILM and BM in a BALB/c mouse with SID (A, B) and SDD (C, D) correction. E–H: axial intensity profiles of ILM and BM in different transverse regions denoted by the corresponding colored arrows (A–D); averaged across 100 images, with SID (E, F) and SDD (G, H) correction. Table I: the full width at half-maximum (mean  $\pm$  std. dev.) of the axial profiles of the ILM and BM in E–H reduce with SDD correction. J–M, Zooms of spectroscopic red–green–blue (RGB) images ( $\lambda_{0,\text{blue}} = 580$  nm,  $\lambda_{0,\text{green}} = 610$  nm,  $\lambda_{0,\text{red}} = 643$  nm) of the ILM (J, L) and BM (K, M) with SID and SDD correction. With SID correction, note the blue “halo” (arrows) above the ILM and below the BM due to non-overlapping sub-bands (J, K). N, P: averaged SDD corrected, spectrally shaped retinal images of C57BL/6 and BALB/c mice with outer retinal image zooms (O, Q). (ILM, inner limiting membrane; ELM, external limiting membrane; IS/OS, inner segment/outer segment junction; OST, outer segment tips; RPE, retinal pigment epithelium; BM, Bruch’s membrane; CC, choriocapillaris; SID, spatially independent dispersion; SDD, spatially dependent dispersion.)

divided the spectrum into seven narrow sub-bands and 10–40 sub-images over a grid of five transverse windows and 2–8 depth windows [Fig. 3(A)]. For each sub-image and sub-band, we calculated a depth shift relative to a reference sub-band [Fig. 3(B)]. The depth shift versus sub-image depth was fit with a first-order polynomial function. The slope corresponded to a scaling of the sub-image due to DDD, while the  $y$  intercept corresponded to a shift due to DID. The slopes and  $y$  intercepts were integrated versus frequency to yield functions for resampling and phase correction, respectively. After a compensation procedure based on phase correction (DID) [6] and resampling (DDD) [8], the sub-bands should overlap and coherently sum to form an ultrahigh resolution OCT image [Fig. 3(B)]. Note that DID varies between subjects due to eye length, while DDD originates from the accumulation of dispersion within the imaging range (as well as possible spectrometer calibration error), which is more consistent across subjects.

To experimentally assess the improvement in image quality achieved by compensating SDD, C57BL/6 and BALB/c mice were imaged *in vivo* (Fig. 4) under isoflurane anesthesia, as approved by our Institutional Animal Care and Use Committee (IACUC). Different dispersion compensation methods were compared [Figs. 4(A)–4(M)] at the ILM and Bruch’s membrane (BM). With spatially independent dispersion (SID) compensation to optimize overall image sharpness, spatial variation in GDD can shift different wavelengths in depth, even over modest axial image depths and fields-of-view of a few hundred  $\mu\text{m}$  [Figs. 4(J) and 4(K)]. Accounting for both transverse and DDD [Figs. 4(C), 4(D), 4(L), and 4(M)], we made axial intensity profiles more uniform across transverse positions [Figs. 4(G) and 4(H)] and reduced their widths [Fig. 4(I)], enabling us to resolve thin retinal bands such as ILM and BM across entire images in both strains [Figs. 4(N)–4(Q)].

In conclusion, we have shown that SDD can degrade performance of visible light OCT, even for apparently modest sample thicknesses of a few hundred  $\mu\text{m}$  and wavelength

bandwidths of  $\sim 100$  nm. Based on observations of DID and DDD shift and depth-scale sub-band images, respectively, we introduced a sub-band, sub-image correlation approach to estimate dispersion parameters. Upon correction of SDD, we resolved fine layers such as the BM and ILM in both non-pigmented and pigmented mice across the entire imaged field-of-view. Our correction method also promises to improve accuracy of spectroscopic OCT.

**Funding.** Glaucoma Research Foundation (GRF); National Institutes of Health (NIH) (NS094681, NS105043, EB023591, EY028287, EY015387).

## REFERENCES

1. F. E. Robles, C. Wilson, G. Grant, and A. Wax, *Nat. Photonics* **5**, 744 (2011).
2. J. Yi, Q. Wei, W. Liu, V. Backman, and H. F. Zhang, *Opt. Lett.* **38**, 1796 (2013).
3. S. P. Chong, T. Zhang, A. Kho, M. T. Bernucci, A. Dubra, and V. J. Srinivasan, *Biomed. Opt. Express* **9**, 1477 (2018).
4. J. J. Hunter, J. I. Morgan, W. H. Merigan, D. H. Sliney, J. R. Sparrow, and D. R. Williams, *Prog. Retinal Eye Res.* **31**, 28 (2012).
5. W. J. Brown, S. Kim, and A. Wax, *J. Opt. Soc. Am. A* **31**, 2703 (2014).
6. M. Wojtkowski, V. Srinivasan, T. Ko, J. Fujimoto, A. Kowalczyk, and J. Duker, *Opt. Express* **12**, 2404 (2004).
7. D. J. Harper, M. Augustin, A. Lichtenegger, P. Eugui, C. Reyes, M. Glösmann, C. K. Hitzenberger, and B. Baumann, *Biomed. Opt. Express* **9**, 2115 (2018).
8. D. L. Marks, A. L. Oldenburg, J. J. Reynolds, and S. A. Boppart, *Appl. Opt.* **42**, 204 (2003).
9. A. G. Van Engen, S. A. Diddams, and T. S. Clement, *Appl. Opt.* **37**, 5679 (1998).
10. W. Choi, B. Baumann, E. A. Swanson, and J. G. Fujimoto, *Opt. Express* **20**, 25357 (2012).
11. S. P. Chong, C. W. Merkle, C. Leahy, H. Radhakrishnan, and V. J. Srinivasan, *Biomed. Opt. Express* **6**, 1429 (2015).
12. B. Cense, N. A. Nassif, T. C. Chen, M. C. Pierce, S.-H. Yun, B. H. Park, B. E. Bouma, G. J. Tearney, and J. F. de Boer, *Opt. Express* **12**, 2435 (2004).